Definition 3.2 and the previous note) or (discrete-time) normalized periodic noise $u_N \in \mathbb{P}_N$ (see Definition 3.3 and the previous note), with maximum angular frequency $\omega_{max} = l_{max}\omega_1$ ($\omega_1 = 2\pi f_1$), we have for $\underset{\sim}{\omega}_L = L\omega_1$, $|L| > l_{max}$:

$$\mathcal{E}\{ Y_L^{\alpha} e^{-j\angle U_l} \} = 0 \tag{3-24}$$

Proof. See Appendix 3.K. □

Note that this theorem is valid for continuous-time and discrete-time systems (using $\underset{\sim}{\omega}$). A direct result of this theorem is that all results of the previous sections can also be applied to discrete-time systems. Because none of the "out-of-band" components can create systematic contributions, the folding process does not change the nature of the output contributions of a nonlinear system, and, hence, the previous proofs remain valid.

3.4.6 Experimental Illustration

A nonlinear mechanical resonating system (mass, viscous damping, nonlinear spring) is simulated with an electrical circuit. The displacement $y(t)$ (output) is related to the force $u(t)$ (input) by the following nonlinear, second-order differential equation:

$$m\frac{d^2y(t)}{dt^2} + d\frac{dy(t)}{dt} + k(y(t))y(t) = u(t) \tag{3-25}$$

The nonlinear spring is described by a static but position-dependent stiffness

$$k(y) = a + by^2 \tag{3-26}$$

For small excitations, the spring becomes almost linear so that the underlying linear system consists of a second-order resonance system. A series of experimental results on this system are shown. First, the nonlinear behavior will be illustrated using stepped sine measurements. Next, the split of the transfer function into the underlying linear system $G_0(j\omega_k)$, the related linear dynamic system $G_R(j\omega_k)$, the stochastic nonlinear distortions $G_S(j\omega_k)$, and the noise contributions $N_G(k)$ are shown.

3.4.6.1 Visualization of the Nonlinearity Using Stepped Sine Measurements. To visualize the nonlinear behavior of the system, a stepped sine measurement is made (Figure 3-4). The frequency of the sine is first stepped upward until the maximum frequency is reached and then stepped down again. At each frequency a measurement is made over an integer number of periods. During the experiment we took care to have a continuous excitation signal; no discontinuities appeared at the frequency-changing instants. The nonlinear behavior of the system is clearly visible. The measured transfer function depends, strongly, on the amplitude of the sine excitation. Moreover, the measurements also show that the actual output of the system depends on the past inputs: the up-path differs from the down-path for large excitations. Such behavior cannot be described using Volterra-based descriptions. Nevertheless, we will still apply the previously developed theory to this system. This can be done because the bifurcation appears only for large excitations, injecting a lot of power close to the resonance frequency of the system. If we use normalized random multisines, only a fraction of the power is injected in this band so that the bifurcation problem does not disturb the measurements anymore.

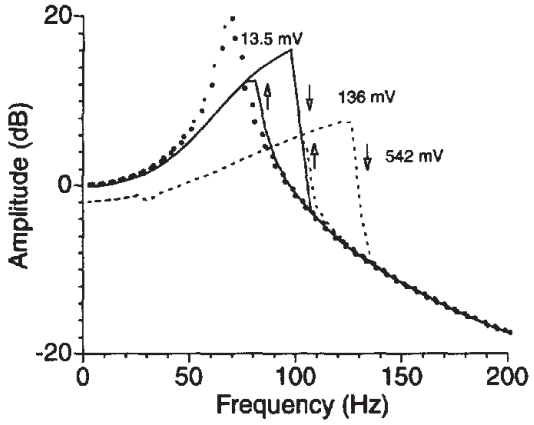

Figure 3-4. Stepped sine measurement at different amplitudes (rms values given). An up and down sweep is made. For the 13.5 mV measurement: black boxes up sweep, white boxes down sweep. For the others: ↓ up sweep, ↑ down sweep.

3.4.6.2 Measurement of the Related Linear Dynamic System. In a second step, the underlying linear system is measured using a normalized random multisine ($f_k = (2k+1)f_0$, $k = 0, 1, \ldots, 1340$ and $f_0 \approx 0.0745$ Hz) with a small amplitude (rms value of 34.2 mV). The standard deviation $\sigma_{N_G}(k)$ is calculated from 10 consecutive periods. The results are shown in Figure 3-5.

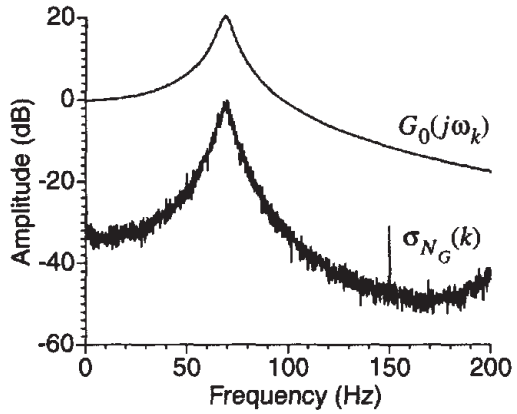

Figure 3-5. Measurement of the underlying linear system $G_0(j\omega_k)$ and its standard deviation.

The impact of the nonlinearity is made visible by increasing the excitation level of the normalized random multisine to an rms value of 127 mV. The measurement was repeated for 10 different realizations of the excitation signal so that $\sigma_{G_S}(k)$ could also be measured. The measurement results are shown in Figure 3-6. On the left side, the related linear dynamic system is compared with the underlying linear system. A number of observations can be made: the resonance frequency is shifted to the right, the peak value is decreased, and the measurement became more noisy.

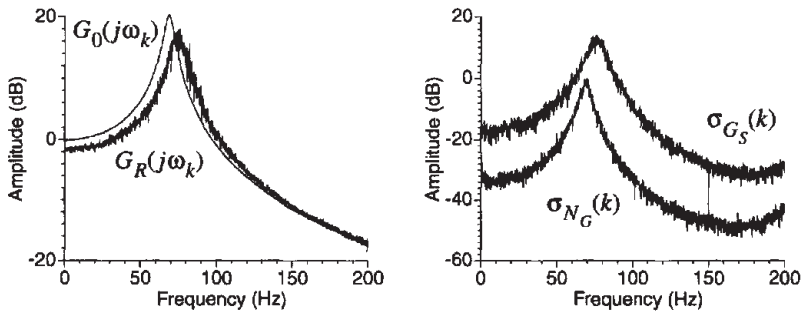

Figure 3-6. Comparison of the measured related linear dynamic system $G_R(j\omega_k)$ obtained from 10 realizations and the underlying linear system $G_0(j\omega_k)$.

The shift to the right of the resonance frequency is due to the nonlinear behavior of the hardening spring. For larger excursions, the average stiffness increases and so also does the resonance frequency. Note that if the $G_0(j\omega_k)$ measurement were not available, there would be no indication at all that this system is strongly nonlinear. This shows, clearly, why we need dedicated tools to detect the presence of nonlinear distortions. The difference between $G_R(j\omega_k)$ and $G_0(j\omega_k)$ is due to the systematic contributions $G_B(j\omega_k)$.

The increased noise level can be understood only from the previous, explained theory; they are due to the stochastic contributions $G_S(j\omega_k)$. Changing the excitation level did not change the disturbing noise, but $G_S(j\omega_k)$ became much larger. This is visualized on the left side of the figure. The standard deviation $\sigma_{G_S}(k)$ is obtained by measuring the FRF from 10 realizations of the normalized random multisine. For the small excitation level, it is completely dominated by the measurement noise $\sigma_{N_G}(k)$, whereas for the large excitation, $\sigma_{G_S}(k)$ dominates. This is also illustrated in Figure 3-7, where the evolution of the measured

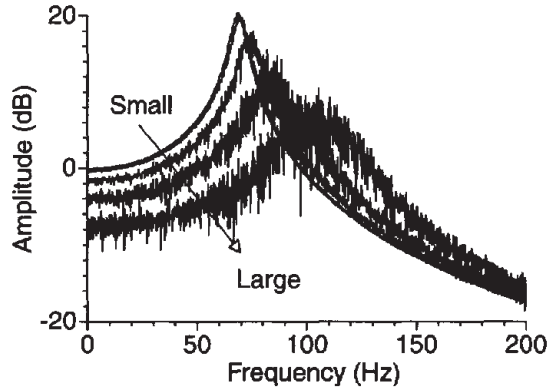

Figure 3-7. Evolution of the related linear dynamic system for growing excitation levels: rms values of 34 mV, 54 mV, 127 mV, 253 mV, and 507 mV.

FRF is shown as a function of the excitation level. As can be seen, the stochastic contributions grow with the level while the measurement conditions (and, hence, the disturbing noise) remain the same. Again, it is very difficult to understand this result without the previously gained insight into the behavior of nonlinear systems. This also suggests a first test to detect the presence of nonlinear distortions. The standard deviation calculated from a set of consecutive periods (without changing the excitation signal) should be the same as that calculated from repeated measurements, using different realizations of the excitation signal.

3.5 DETECTION OF NONLINEAR DISTORTIONS

The ideal FRF-measurement method should provide the measured FRF, and at the same time the presence of nonlinear distortions should be detected, qualified (even or odd distortions), and quantified (the level of the distortions). Because the prime interest in these measurements is the FRF, it is unacceptable that most of the time would be spent on the detection of the nonlinear distortion at the cost of a reduced quality of the FRF measurement. This excludes most existing methods that require a series of dedicated measurements to make the nonlinearity test. In general, it is impossible to realize this ideal; however, when specially selected periodic excitations are applied, we can come close to it. This will be shown in the next section. Finally, in Section 3.5.3 some background information on the classical detection methods is given.

3.5.1 Detection of Nonlinear Distortions Using Periodic Excitations

The sine test is the simplest test characterizing, directly, the nonlinear behavior by verifying the generation of higher harmonics. However, this approach has a number of serious drawbacks. It is not only very slow (see Chapter 2), but as shown in the example of Section